

Photosystem II network benefits from mixed chlorophylls in the antennae

Heetae Kim^{1,5*}, Eunchul Kim^{2,3,5}, Mauricio Vargas⁴, Jun Minagawa³⁺

¹ Data Science Institute, Universidad del Desarrollo, Santiago, 7610658, Chile

² Division of Biological Science, Graduate School of Science, Nagoya University, Nagoya

³ National Institute for Basic Biology, 38 Nishigonaka, Myodaiji, 444-8585, Okazaki, Japan

⁴ Instituto de Matemáticas, Universidad de Talca, Casilla 747, Talca, Chile

⁵ These authors contributed equally to this work

* heetaekim@udd.cl +minagawa@nibb.ac.jp

Photosynthesis is the primary energy production process of ecosystem. Throughout the green plants, two different types of chlorophylls, Chl-*a* and -*b*, are bound to the light-harvesting complex for photosystem II. While the structure and functional characteristics of the two types of chlorophylls have been well documented as individual, the features of the coexistence has yet to be understood clearly. Here, we present a principled framework for discerning and quantifying the chlorophylls' role during the excited energy transfer. Our approach combines network science^{1,2} and Monte Carlo Markov analysis based on the Förster resonance energy transfer rates³ between all the chlorophyll pairs in the light-harvesting antennae for photosystem II. We find that the excitation energy can be rapidly confined to the specific chlorophyll clusters in the light-harvesting complex, where excess energy dissipation possibly takes place, only when both chlorophyll species are involved. Comparing to other models with hypothetical chlorophyll compositions, we show that the light harvesting system with natural chlorophyll *a* and *b* ratio is the most advantageous for the photosystem II supercomplex to balance the light-harvesting and photoprotection capabilities.

In oxygenic photosynthesis, the chlorophylls (Chls) embedded in the photosystem II (PSII) supercomplex (SC) perform a major role of photosynthesis by absorbing light and transferring the excited energy to the reaction centers (RCs) where charge separation occurs, initiating electron flow for CO₂ fixation⁴. In green plants, the PSII SC comprises two functional groups of proteins: the core complex containing RCs and the peripheral light-harvesting complexes (LHCII)⁵. The core complex possesses a single type Chl *a*, whereas LHCII includes two distinct Chls, Chls *a* and *b*. As Chl *b* has a higher energy level than Chl *a*, the coexistence of Chls *a* and *b* causes a unidirectional energy stream from Chl *b* to Chl *a*⁶. If the LHCII only binds Chl *b*, the excited energy would be most utilized for charge separation at RCs, which only binds Chl *a*. Although this ‘all-*b*’ system seems to be advantageous for photosynthesis, the natural light-harvesting antennae bind both Chl *a* and *b* throughout the green plants. The reason why the natural light-harvesting antennae adopt the mixed Chl system has, however, yet to be understood clearly. In what follows, we make our claim rigorous by introducing complex network analysis¹ that has been successfully applied to various complex systems^{7–12}, and shed light on the connection between the energy transfer dynamics and the topological characteristics of PSII SC to decipher an advantage of the nature’s complex system.

The energy transfer network of the PSII SC (PSII network) constructed in this study consists of nodes and links that correspond to Chls and energy transition probability between Chls, respectively. The coordinates and the orientation of transition dipoles for each Chl are obtained from the molecular structure of the PSII SC¹³ (Fig. 1a, red dashed arrows for Chls A611 and A603 in protein ‘4’ as an example). The distance and the angle between each pair of transition dipoles are then utilized to calculate Förster resonance energy transfer (FRET) rates between the Chls (Fig. 1a, navy arrow). In this study, we applied the FRET equation for the rate

constant of the excited energy transfer to look through the overall trend of the excited energy dynamics in whole PSII SC by assuming non-coherent and dipole-to-dipole energy transfer models¹⁴ (see Method section ‘FRET rate calculation’). To investigate more realistic excited energy dynamics, including excitonic coupling effects between pigments will be required¹⁵.

Based on the FRET rates we constructed a transition rate matrix $\mathbf{Q}^{16, 17}$ of PSII SC, and then converted it to the transition probability matrix \mathbf{P} (See Method section ‘Excitation energy transfer simulation’). The matrix \mathbf{P} for the entire PSII SC is in Fig. 1c with its element p_{ij} indicating the probability of transferring the excited energy from a Chl site i to j ¹⁸. It reveals the characteristic excited energy transition pattern of PSII SC, that is, the transition probability between Chls is not evenly distributed but clustered by proteins (Fig. 1c).

We mapped the transition probability as the link weight of the PSII network as shown in Fig. 1d. In the PSII network, LHCII_s are placed in the peripheral area and the RCs are located at the center of PSII SC. We also systematically constructed the PSII network models by varying the ratio between Chl *a* and Chl *b* in LHCII for a comparative analysis. The natural type represents the PSII SC with the natural LHCII, where Chl *a*/*b* is approximately 3/2, whereas all-*a* type (or all-*b* type) has hypothetical LHCII only binding Chl *a* (or only Chl *b*). The other models are constructed by altering the ratio of the two types of Chls in either major or minor LHCII (see Method section ‘Network analysis on PSII network models’ and Extended Data Fig. 1). The PSII network models were used to estimate quantum efficiencies for photosynthesis (charge separation) of the PSII SC. By applying empirically obtained rate constants ($1/1.5 \text{ ps}^{-1[19]}$ and $1/2.0 \text{ ns}^{-1[20]}$, respectively) for charge separation at the special pair and intrinsic decay of Chls’s excited states in the thylakoid membrane, we obtained the probability of excitation tendency of various types of PSII networks when the fluctuation was less than 10^{-7} . The quantum efficiency

for photosynthesis of the natural type PSII network was thus estimated as about 0.86. It well coincides with the empirical quantum yield of PSII (0.75–0.87^{21–23} and another estimated quantum yield in analytical way²⁴ (see Method section ‘Analytic yield estimation’). On the other hand, the quantum efficiencies for photosynthesis of all-*a* and all-*b* type PSII were estimated as about 0.73 and 0.92, respectively. These results show that the quantum efficiency for photosynthesis of the PSII RC depends upon the Chl compositions.

To investigate the excited energy transfer dynamics in PSII networks, we estimated the excitation probability of Chls in each model. The excited energy transition process is independent of the past events, and is decided only by the current states, which satisfies Markov property²⁵. Assuming that all Chls can be initially randomly excited, we calculated the average excitation probability. We call the normalized average excitation probability as excitation tendency $\rho_i(t)$. The excitation tendency estimates the probability of holding the excited energy on each Chl, and it can be used to calculate the quantum yield of photosynthesis (see Method section ‘Excitation energy transfer simulation’).

The excitation tendency can reveal the temporal dynamics of the energy transfer process as it discloses the different time intervals between intra- and inter-protein energy transition of the natural PSII network (Figs. 2a and 2b). For example, Fig. 2a and 2b show the natural PSII network and the time series of the excitation tendency of the Chls. We found that the excitation tendency was not evenly distributed among Chls, and there existed a notable separation between Chl *a* and Chl *b*. One can see that Chls *a* accumulate energy resulting in the peaks of excitation tendency curves (Fig. 2b purple), while the other Chl *b* and RCs hold low tendency (Fig. 2b orange and green). It means that in natural PSII network the excited energy in Chl *b* is rapidly redistributed to Chl *a* in a short time scale forming the intraprotein transfer regime (Fig. 2b,

shading). On the other hand, the energy transfer between proteins slowly follows after the intraprotein transfer. Fig. 2c shows the protein network of the PSII SC—each node is a group of Chls in a protein—and Fig. 2d shows the average excitation tendency per protein. For the entire transition process, the RCs (the proteins ‘A’ and ‘D’) consistently show the lowest tendency, since the energy is immediately used for charge separation. One can see that the transition shapes of the excitation tendency of proteins vary especially during the interprotein transfer regime (Fig. 2d, shading). The different time intervals between the intra- and inter-protein transfer regimes provides us a clue that in the natural PSII SC the excited energy is redistributed within each protein at first and then transported to other proteins.

Interestingly, some specific Chls exhibited exceptionally high excitation probability during the energy transition. For instance, see the cropped network structure of a protein ‘2’ (an LHCII subunit in M-trimer) in Fig. 2e, and the temporal behavior of the excitation tendency of the involved 14 Chls in Fig. 2f. The most probable Chl to be excited in the protein ‘2’ is the Chl A604 that gets higher tendency more than twice of the random case (dashed grey line). The snapshots of the temporal dynamics of the protein ‘2’ is shown in Fig. 2g as a network structure with the node size proportional to the excitation tendency. In the beginning ($t=1\times10^0$), the excitation tendency is evenly distributed among Chls *a* and *b*. The downhill transfer from Chl *b* to Chl *a* causes the unequal distribution between Chls *a* and *b* during the transition process (see $t=3\times10^1$ and 1×10^3). In this period the excited energy is concentrated in some specific Chls *a* (such as A604 in the protein ‘2’ for example) and managed afterward. In the long run, the excited energy is transferred out of the protein and all Chls have very low chance to be excited ($t=3\times10^4$).

The distinct time scale between intra- and inter- protein transfer regimes was not observed when the PSII SC lacks the diversity of Chl *a* and *b* in LHCII. In particular, in the all-*a* type PSII network where only Chl *a* exists in the entire PSII SC, the transition patterns of the excitation tendency of Chls and proteins were identical except for RCs due to the absence of the downhill stream as shown in Figs. 3a and 3b, respectively. The excitation tendency of all-*a* type PSII network was maintained lower than the random initial tendency for all Chls for all the time. It implies that in an LHCII with single-type-Chl, the excited energy is rather diffused than systemically transported.

Unlike all-*a* type, the other extreme case, all-*b* type, showed the diverse excitation tendency distribution among Chls (Fig. 3c) or proteins (Fig. 3d). However, in both all-*a* and all-*b* types the hierarchical energy transfer from intra- to inter- protein transition was not observed as the separated regimes as in the natural type PSII network, where the step-by-step energy transfer occurs from local Chls through the neighboring proteins, and finally to the RCs (Fig. 2). The heterogeneous excitation tendency between Chls specifies the systematic energy transition process of PSII SC.

An important remark is that the excitation tendency of the core proteins ('A' and 'D' in Fig. 3d) initially decreased, but then reverted. This is because the energy transferred from the peripheral Chls to the core proteins was gathered at a faster rate than the charge separation, such that it increased over-charging risk of core proteins. We discuss this later.

To estimate the heterogeneity of the excitation tendency distribution, we calculated Gini index to provide a measure of the inequality of distribution. The Gini index is measured by using a cumulative probability distribution function of a wealth, called Lorenz curve^{26, 27}. When a commodity is equally distributed, the Lorenz curve becomes a straight line showing that the

linear increase of the amount of the distributed commodity according to the population. The Gini index, $g(t)$, is the relative proportion of the area over the Lorenz curve to the equal distribution line (inequality gap), such that the index is between 0 for the equal distribution (all agents have the same amount of certain commodity) and 1 for the extremely unequal case (an agent has all and the others have nothing).

From the dynamics of the calculated Gini index of the excitation tendency of Chls, we found that the natural PSII network showed the fastest increase of the excitation inequality comparing to the all-*a* or all-*b* types (Fig. 4a). The rapidly established high Gini index of the natural type tells us that the energy transfer paths are rapidly formed through specific Chls. Specifically, some Chls in LHCII consistently had high excitation tendency during the transfer process (see the red colored nodes in Fig. 4b). On the other hand, the all-*a* type model— that lacks the downhill gradient—consistently showed low Gini index effectively indicating the identical excitation tendency distribution among all Chl *a* (Fig. 3a). The Gini index of the all-*b* type model followed the all-*a* type in the beginning, but in the long run (around at $t > 5 \times 10^3$) it increased even higher than that of the natural type (Fig. 4a). Nonetheless, the spatial distribution pattern in all-*b* type was opposite to the natural type: the high-excitation-tendency nodes were not in the periphery (LHCII) but in the core (Fig. 4d) due to the global downhill gradient from LHCII to the core area. Recall that the incoming rate to the cores here is faster than the charge separation rate. It caused the excessive energy concentration at the RCs (proteins ‘B’ and ‘C’ in Fig. 3d) bringing about the photodamage risk at these sites.

The other types that also have both Chl *a* and Chl *b* in LHCII, including major *a*-, minor *a*-, major *b*- and minor *b*-types showed that the excessive excited energy confined in part of LHCII was not as efficient as the natural type (Extended Data Figs. 1 and 3). It means that

natural PSII SC (Chl $a/b = 3/2$) can be superior to the other types of composition of Chls a and b , in terms of the photodamage risk management.

When the excessive energy wanders in LHCII, it most likely comes across the photodamage protectors that are known as non-photochemical quenchers^{28–30}. We identified the topologically central Chls in the natural PSII network while the excited energy jumps from one of the Chls to another. We investigated all origin-destination pairs of Chls to estimate the randomized shortest path (RSP) betweenness centrality of each Chl^{1,2}. The RSP betweenness centrality of a Chl is the normalized number of energy transfer paths—both the shortest and random detours—laying over the Chl (see Method section ‘Network analysis on PSII network models’). We found that the Chls in the RCs have the highest RSP betweenness centrality because they are located at the central area of the network with limited connections. Therefore, the RCs are so-called bridges (or gateways) where the excited energy should pass through to travel between both sides (Fig. 5a, the nodes with green edge stroke).

More importantly, there also exist some high-betweenness Chls in the peripheral area of the PSII network. It means that when the excited energy is confined in LHCII by the aforementioned energy transfer dynamics, it will more likely pass through those high-betweenness Chls in the area. We found that most of those high-betweenness Chls in LHCII were the excitonically coupled Chl cluster A610-A611-A612 in LHCII trimers^{28, 29} and Chl dimer A603-A609 in CP29³⁰ (Fig. 5a, the nodes with blue link stroke). Intriguingly, these Chls have been proposed as quenchers for the non-photochemical quenching (NPQ)-dependent photoprotection (Fig. 5a, the nodes with blue link stroke). Therefore, the induced distribution of the excited energy in the LHCII—driven by the coexistence of Chls a and b —possibly enables

the PSII SC to execute the excess energy dissipation effectively when it is necessary, as if one puts fire near to firefighters.

The yield of the excited energy transfer was enhanced when we increased the proportion of Chl *b* in LHCII, which induced more gradient to the core-protein region (Fig.5b). When the LHCII was fully filled with Chl *b* (all-*b* type), the excited energy was most utilized for charge separation at RCs. Therefore, the all-*b* type can be on one hand advantageous for photosynthesis especially in the low light conditions. However, it can also be dangerous on the other especially in the high light conditions because the excessive energy in the core-proteins could cause photodamage. The natural type PSII, however, seems to have a safe, yet efficient characteristics. The path of the excitation energy transfer is structured to prevent itself from photodamage as shown by the high Gini index and the location of the high-betweenness Chls. Among various types of PSII networks with different proportion of Chl *b* (from 0% to 100% of LHCII, Fig.5b and Extended Data Fig. 1), the natural type showed the highest Gini index at early time and moderate efficiency. It suggests that the natural conformation of Chls *a* and *b* in LHCII may reflect the optimal configuration providing the balance between security and efficiency.

Previous research on the excitation transfer dynamics in photosynthesis has been carried out with a simplified analysis limited to the distances between Chls¹³ as well as the orientation of Chls^{14,31} due the technical limits of quantum mechanical treatments considering coherent and coupling effects of each Chl^{28, 32}. In this study, we have considered the PSII SC as a whole mapping it into a complex network. From the probabilistic energy transfer process and the topological nature of the PSII network, we have revealed that the natural LHCII with both Chls *a* and *b* is beneficial to the PSII SC. We have taken steps towards understanding the photosystem from the network point of view, but its full potential remains unexplored. Our work has primarily

focused on the topological betweenness and transmission dynamics of the PSII network, but other network science approaches such as community characteristics and resilience analysis as well as fusion with quantum mechanical treatments hold great promise for further study.

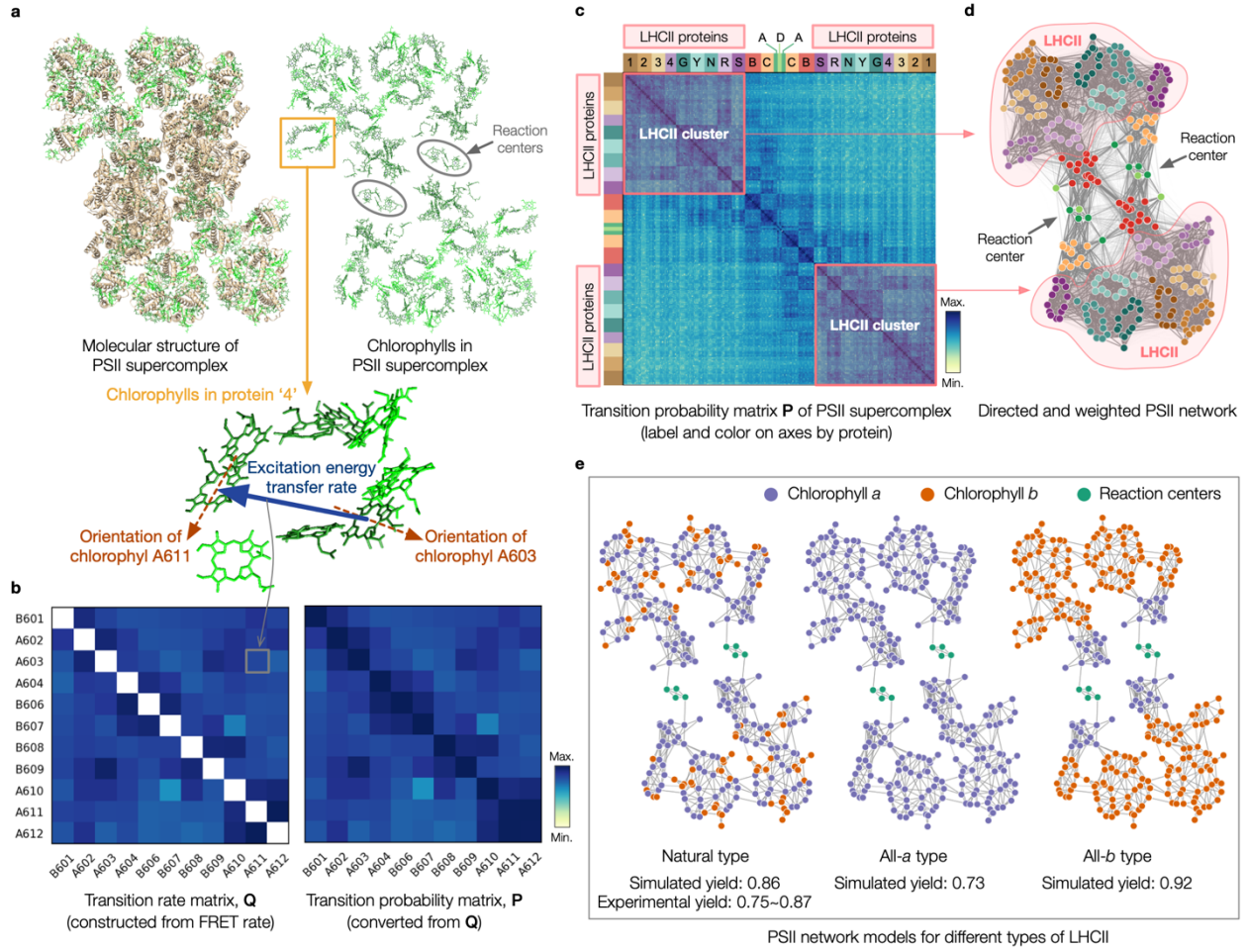


Fig. 1 | Construction scheme of PSII networks from the molecular structure of PSII SC. (a)

The angle and distance between Chls are converted to (b) the energy transfer rate and the probability of the transition. The transition probability matrix P (c) is converted to the corresponding PSII network in (d). Here the node colors in (d) represent the protein groups matching the label colors of P in (c). Only top 20% links are shown for a legible visualization.

Varying the composition of LHCII, various PSII network models are constructed for a comparative analysis (e, top 2% links are shown).

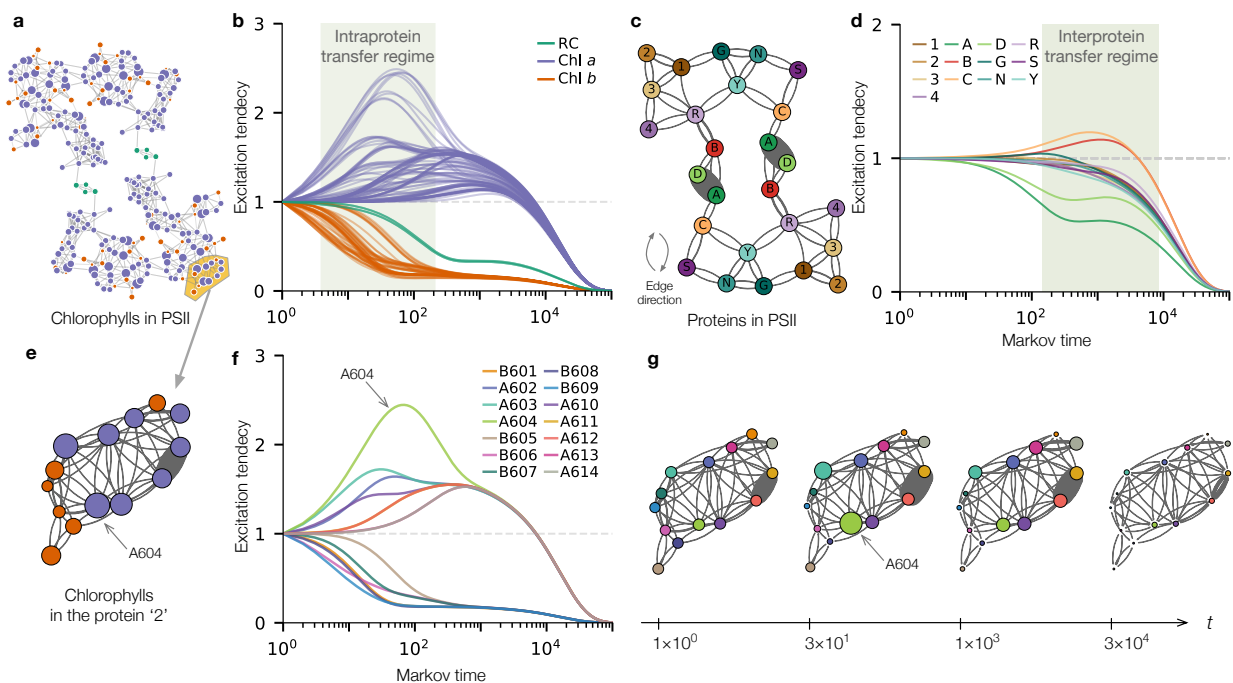


Fig. 2 | The temporal dynamics of the excitation tendency of the natural PSII network. (a) The natural PSII network consists of Chl *a* (purple), Chl *b* (orange), and RCs (green), and (b) the time series of the excitation tendency shows the distribution change over time. The transition dynamics by proteins in PSII SC (c) shows that the unequal distribution between proteins (d) indicating that the interprotein energy transfer (shading in d) occurs later than the intraprotein transfer (shading in b). The Chls of a protein '2' (e) undergo the excitation tendency fluctuation (f) as shown in the snapshots at each time (g).

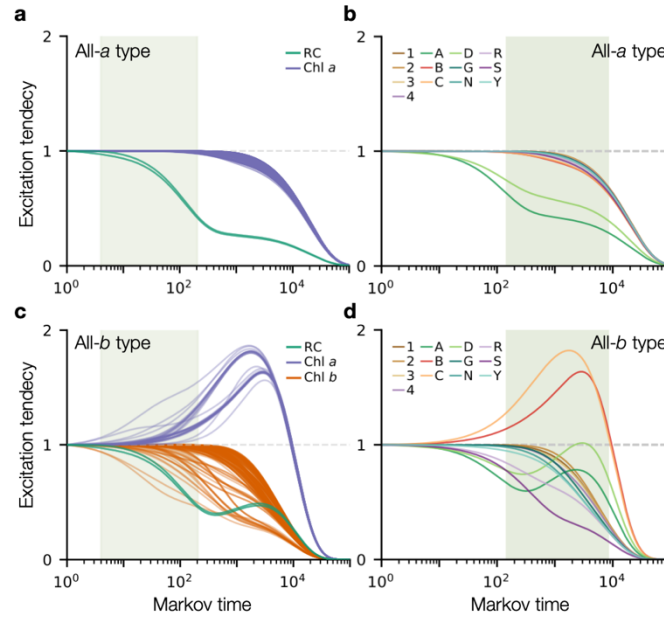


Fig. 3 | The temporal dynamics of the excitation tendency of all-*a* and all-*b* type PSII networks. The excitation tendency of Chls for all-*a* or all-*b* type is shown in (a) or (c), and the dynamics of proteins is in (b) or (d), respectively.

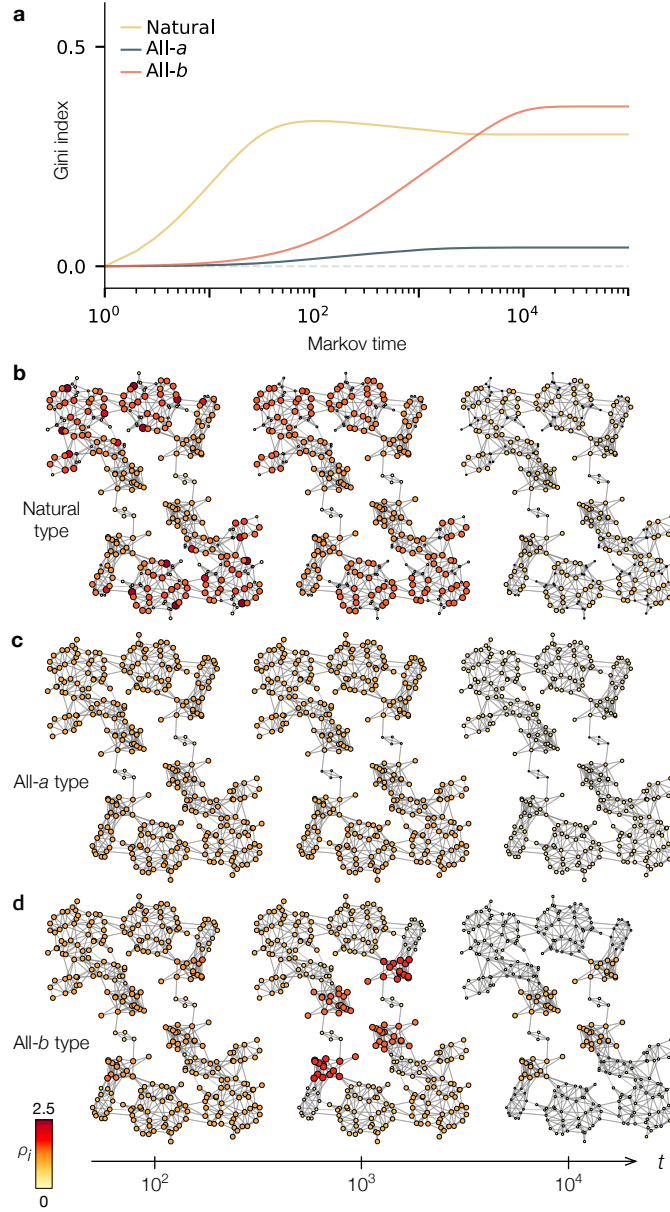


Fig. 4 | The time series of Gini index and the spatial distribution of the excitation tendency in various PSII networks. (a) The Gini index of three types of PSII networks. (b–d) The excitation tendency of Chls in natural type (b), all-*a* type (c), and all-*b* type (d) PSII networks at $t=10^2$, 10^3 , and 10^4 .

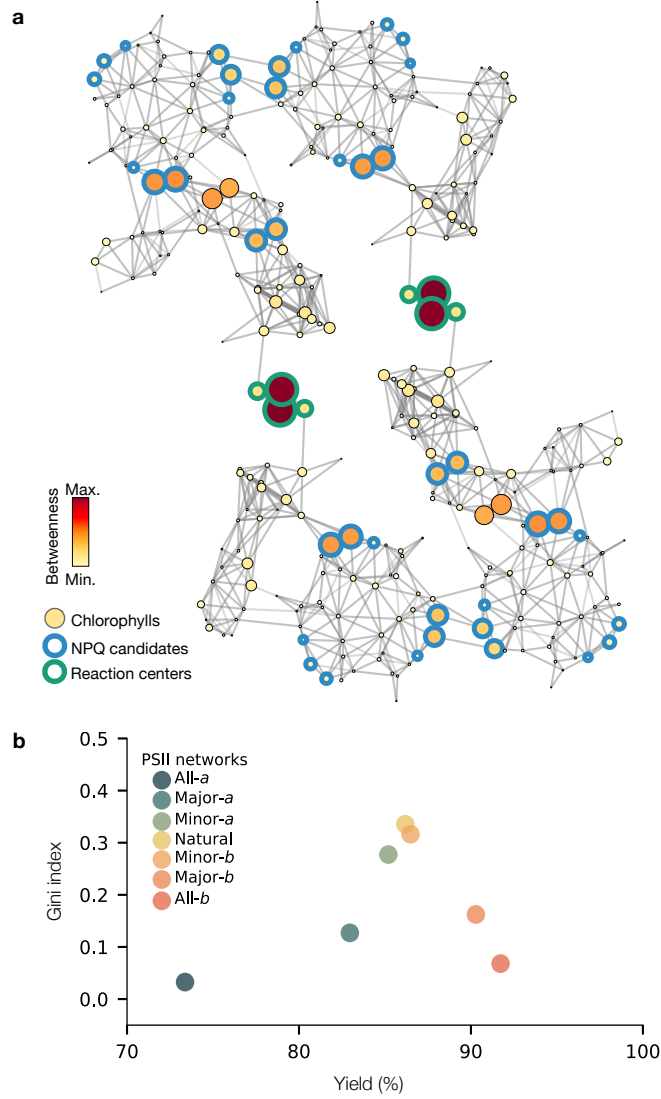


Fig. 5 | The RSP betweenness centrality of the Chls in the natural PSII network and the Gini index with the simulated yield at $t=10^5$ of various PSII networks. (a) the high-betweenness nodes are frequently observed in the RCs (nodes with green stroke) or the photoprotection units (nodes with blue stroke). (b) Among the various models, the natural PSII network shows the highest Gini index at $t=10^2$ and intermediate level of yield at $t=10^5$.

Method

FRET rate calculation. FRET rate constant between two Chls i and j is defined based on the FRET theory as described previously^{14,31}: $\lambda_{ij} = (c\kappa^2)/(r^4d^6)$, where c is the factor calculated from the spectral overlap integral between the Chls. The values vary according to the type of Chls in the origin and destination. We used 32.26 for Chl $a \rightarrow$ Chl a , 1.11 for Chl $a \rightarrow$ Chl b , 9.61 for Chl $b \rightarrow$ Chl a , and 14.45 for Chl $b \rightarrow$ Chl b ⁶. The dipole orientation factor κ^2 is calculated by $\kappa^2 = [\hat{u}_D \cdot \hat{u}_A - 3(\hat{u}_D \cdot \mathbf{R}_{DA})(\hat{u}_A \cdot \mathbf{R}_{DA})]^2$, where \hat{u}_D and \hat{u}_A are the dipole unit vectors of donor and acceptor Chls, respectively, derived from the vectors from the coordinates of NB and ND atoms of respective Chls. \mathbf{R}_{DA} is the unit vector of the vector from the magnesium atom of the donor Chl and to the magnesium atom of the acceptor Chl. r is the refractive index that we use 1.55⁶. d is the distance between magnesium atoms of donor and acceptor Chls. The protein structure (PDB: 5xn1¹³) of a plant PSII–LHCII supercomplex were used to generate FRET rates network of a PSII–LHCII supercomplex and the FRET rates were computationally calculated using a custom-made algorithm¹⁴ on the Python platform (Python v.3.6).

Excitation energy transfer simulation. The consecutive excitation energy transfer is initiated at one of the Chls and terminated when the excitation energy is utilized for charge separation at special pairs in RCs (photosynthesis) or intrinsically dissipated. We denote the set of the transient states of the total 314 Chls as $T = \{i | i \leq 314\}$ and two absorbing states representing the charge separation and dissipation as $A = \{i | i = 315, 316\}$. Representing the possible states S at each transition, the number of states $|S| = |T| + |A| = 314 + 2 = 316$. In the photosystem, for all time $t \geq 0$ and all possible states i_0, \dots, i, j , the excited energy transition process is a stochastic process that follows $\mathbb{P}(\mathbf{x}_{t+1}=j | \mathbf{x}_t=i, \mathbf{x}_{t-1}=i_{t-1}, \dots, \mathbf{x}_0=i_0) = \mathbb{P}(\mathbf{x}_{t+1}=j | \mathbf{x}_t=i) = p_{ij}$ such that it satisfies the Markov

property^{16,17}. Therefore, we generate the transition rate matrix $\mathbf{Q} \in \mathbb{R}^{|S| \times |S|}$ (also known as generator matrix) from the excited energy transition as a Markov process^{15,16}. Assuming $\mathbf{x}(t_0) = i \in T$, for the first-order reaction of the excited energy transfer during photosynthesis, where the transition jump continues to the next state $j \in T$ at $t_1 \sim \exp(\lambda_{ij})$, one can approximate the transition rate from the FRET rate such that $q_{ij} \approx \lambda_{ij}$. Similarly, the rate constant of charge separation in RCs is set as $q_{ij} = 1/1.5 \text{ ps}^{-1[19]}$, where i is the particular Chl in RCs and $j=315$, while the dissipation is set identically for all Chls $q_{ij} = 1/2.0 \text{ ns}^{-1[20]}$, where $i \in T$ and $j=316$. Note that the transient states ($i \in T$) represent the distinct Chls in PSII that are physically exist, whereas the two additional absorbing states ($i \in A = \{315, 316\}$) are conceptual. The diagonal elements are set as $q_{ii} = -\sum_{j \neq i} q_{ij}$ considering that no self-transition occurs. We then convert the transition rate matrix of PSII to the embedded discrete-time Markov chain, $\mathbf{P} = \mathbf{I} - \mathbf{Q}/l$, where \mathbf{I} is the identity matrix and l is the smallest element of the diagonal of \mathbf{Q} , $l = \min(q_{ii})$ ¹⁸. The elements of \mathbf{P} , p_{ij} , indicate the probability of transferring the excitation energy between states. We consider the excited energy transition between S states such that $\sum_{j=1}^S p_{ij} = 1$ for all i .

Upon giving the initial conditions of the states, one can numerically track the transition process of the excited energy by multiplying \mathbf{P} . Let the vector $\mathbf{x}(t) = [x_1(t), x_2(t), \dots, x_{316}(t)]$ be the state vector indicating the excitation probability of each state i at Markov time (or step) t . Since the vector represents the probability distribution, at all Markov time t it satisfies $\sum_{i=1}^S x_i(t) = 1$. We let a Chl i be initially excited by defining the i -th element $x_i(0)=1$ and $x_{j \neq i}(0)=0$ otherwise in the initial state vector $\mathbf{x}(0)$. The excited energy can move to the next state following the transition probability $\mathbb{P}(\mathbf{x}(t+1)=j | \mathbf{x}(t)=i) = p_{ij}$, such that the next states $\mathbf{x}(1)=\mathbf{x}(0)\mathbf{P}$; $\mathbf{x}(2)=\mathbf{x}(1)\mathbf{P}=\mathbf{x}(0)\mathbf{P}^2$; \dots ; $\mathbf{x}(t)\mathbf{P}=\mathbf{x}(0)\mathbf{P}^t$. In this sense, one can recursively estimate the probability distribution at any t -th step. Note that $\mathbf{x}(0)\mathbf{P}^t$ depends on the initial distribution of $\mathbf{x}(0)$. We

assume that only a chlorophyll is initially excited, and no additional excitation occurs during the Markov process. In order to estimate the average probability distribution over the initial target Chls, we take the ensemble average over i , such that $\bar{\mathbf{x}}(t) = \sum_i^T p_i \mathbf{x}_{(i)}(0) \mathbf{P}^t$, where p_i is the initial excitation probability of Chl i . In this study we assume that all Chls can be randomly excited such that $p_i = 1/|T| = 1/314$. Therefore, we estimate the average probability distribution for PSII as $\bar{\mathbf{x}}(t) = \frac{1}{|T|} \mathbf{x}_T(0) \mathbf{P}^t$, where $\mathbf{x}_T(0) = [1, 1, 1, \dots, 1, 1, 0, 0]$ with $x_i = 1$ for $i \in T$ or 0 for $i \in A$. We further normalize $\bar{\mathbf{x}}(t)$ by the random probability, $1/314$, to analyze the probability distribution relatively to the random event. We call the normalized average excitation probability of Chls as excitation tendency $\rho_i(t) = 314 \times \bar{\mathbf{x}}(t)$. The excitation tendency per protein is the average of that of Chls: $\rho_p(t) = \langle \rho_{i \in p}(t) \rangle$, where p is the protein index.

Analytic yield estimation. The steady states solution of $\bar{\mathbf{x}}(t)$ indicates the expected yield of the photosynthesis and loss from the dissipation of PSII network. We use the canonical form \mathbf{P}^* of the Markov chain to calculate the absorbing distribution²⁴:

$$\mathbf{P}^* = \begin{bmatrix} \mathbf{T} & \mathbf{R} \\ \mathbf{0} & \mathbf{I} \end{bmatrix},$$

where $T \in \mathbb{R}^{|T| \times |T|}$, $R \in \mathbb{R}^{|T| \times |A|}$, $0 \in \mathbb{R}^{|A| \times |T|}$, and $I \in \mathbb{R}^{|A| \times |A|}$. In absorbing Markov chain, the transfer always ends in one of the absorbing states. One can estimate the probability, b_{ij} , of the transfer chain that is started from the transient state $i \in T$ and terminated in one of the absorbing states $j \in A$ from the absorbing probability matrix $\mathbf{B} \in \mathbb{R}^{|T| \times |A|}$. To get $\mathbf{B} = \mathbf{FR}$, we use the fundamental matrix $\mathbf{F} = (\mathbf{I} - \mathbf{S})^{-1} \in \mathbb{R}^{|T| \times |T|}$. The row vector $\mathbf{c}_{(i)} \in \mathbb{R}^{1 \times |T|}$, where the i -th Chl is excited with $c_i = 1$ and 0 otherwise, defines the initial excitation probability. Then, the absorbing probability corresponding to the initial excitation at i is calculated from the vector

$\mathbf{y}_{(i)} = \mathbf{c}_{(i)} \mathbf{B} \in \mathbb{R}^{1 \times |A|}$. The average yield and loss are then the ensemble average for all possible random initial excitation at Chls: \bar{y}_1 and \bar{y}_2 , respectively.

Gini index. We characterize the excitation tendency distribution by using the Gini index²⁷. The Gini index (g , also known as Gini coefficient) originally developed to measure the inequality of wealth or income distribution. In this study, however, we apply it to quantitatively analyze the heterogeneity of the excitation energy distribution. To estimate the Gini index, we use the Lorenz curve that is the cumulative probability distribution as a function of the cumulative population²⁶. When the excitation tendency is identical for all chlorophylls, the cumulative probability linearly increases as a function of the number of Chls generating a straight line: a perfect equality. Let g_a be the area between the equality line and the Lorenz curve and g_b be the area under the Lorenz curve. The Gini index is then $g = g_a / (g_a + g_b)$. In extreme situations, $g = 0$ when all chlorophylls have the same excitation tendency, and $g \approx 1$ when only a chlorophyll has 100% of the excitation probability.

Network analysis on PSII network models. We convert the natural PSII SC into a network structure—we call natural PSII network—with nodes representing the Chls in PSII and links for the energy transfer rate between the pairs of them. The spatial coordinates of Chls remain in the PSII network, and the directed link weight from node i to j is identical to p_{ij} in \mathbf{P} . Therefore, the PSII network is a directed and weighted fully connected spatial network for the total number $n = |T| = 314$ of nodes and the total number $m = n(n-1) = 98,282$ of links. The PSII network is in principle a fully connected network between all pairs of Chls, since the energy transfer rate between Chls are all positive values. However, considering the fact that the energy transfer rate

decays exponentially fast—inversely proportional to the sixth power of the distance between Chls—one can filter out the links with negligible low weight remaining a backbone of the network. In this study we estimate the centrality and energy transfer dynamics based on the fully connected relationship while we visualize the network with only some part of all links for visual clarity.

In the PSII network, where the excited energy transfers between Chls probabilistically proportional to the FRET rate, betweenness centrality can reveal the functionally central Chls in the system. Formally, the betweenness centrality of node i is defined by the number of paths starting from node s and ending in node t that go through node i over all s - t pairs. Therefore, it reveals the topologically central nodes that are most positioned on the connecting paths between pairs of nodes. When analyzing the connecting path, it is convenient to consider either the shortest path or random walk. We utilize the randomized shortest paths (RSP) betweenness centrality² that enables us to count both types of paths with a tuning parameter β . With $\beta = 0$ or ∞ one gets the RSP betweenness centrality identical to the random-walk betweenness centrality or shortest path betweenness centrality, respectively. We use the MATLAB code provided² for the betweenness estimation with $\beta=0.1$.

For the comparative analysis, we construct various types of the PSII network models besides the natural PSII network. By alternating Chl b to Chl a (Chl a to Chl b) in LHCII of the natural PSII network, we generate all- a type (all- b type) PSII network that has only a single type Chl in LHCII. We also construct the intermediate versions of PSII networks between those models by partially modifying chlorophylls. Specifically, we change the Chls only for those that are in minor or major components in LCHII. By this, we prepare total seven distinct PSII networks varying the composition of the Chl types (see Extended Data Fig. 1).

Data availability The data/reanalysis that support the findings of this study are publicly available online: https://github.com/heetae/PSII_network_analysis

Code availability The Python code used for the analysis is available on GitHub (https://github.com/heetae/PSII_network_analysis).

References

1. Newman, M. E. J. *Networks: An Introduction*. (Oxford University Press, 2010).
2. Kivimäki, I., Lebichot, B., Saramäki, J. & Saerens, M. Two betweenness centrality measures based on Randomized Shortest Paths. *Sci. Rep.* **6**, 1–15 (2016).
3. Förster, T. Ein beitrage zur theorie der photosynthese. *Z. Naturforsch.* **2b**, 174–182 (1947)
4. Blankenship, R. E. *Molecular Mechanisms of Photosynthesis* (Wiley-Blackwell, New Jersey, 2014).
5. Dekker, J. P. & Boekema, E. J. Supramolecular organization of thylakoid membrane proteins in green plants. *Biochim. Biophys. Acta* **1706**, 12–39 (2005).
6. Gradinaru, C. C. et al. The flow of excitation energy in LHCII monomers: implications for the structural model of the major plant antenna. *Biophys. J.* **75**, 3064–3077 (1998).
7. Albert, R., Jeong, H. & Barabási, A.-L. Internet: Diameter of the World-Wide Web. *Nature* **401**, 130–131 (1999).
8. Strogatz, S. H. Exploring complex networks. *Nature* **410**, 268–276 (2001).
9. González, M. C., Hidalgo, C. A. & Barabási, A.-L. Understanding individual human mobility patterns. *Nature* **453**, 779–782 (2008).
10. Clauset, A., Moore, C. & Newman, M. E. J. Hierarchical structure and the prediction of missing links in networks. *Nature* **453**, 98–101 (2008).
11. Avena-Koenigsberger, A., Misić, B. & Sporns, O. Communication dynamics in complex brain networks. *Nat. Rev. Neurosci.* **19**, 17–33 (2018).
12. Boers, N., Goswami, B., Rheinwalt, A. et al. Complex networks reveal global pattern of extreme-rainfall teleconnections. *Nature* **566**, 373–377 (2019).
13. Su, X. D. et al. Structure and assembly mechanism of plant C₂S₂M₂-type PSII-LHCII supercomplex. *Science* **357**, 816–820 (2017).
14. Sheng, X. et al. Structural insight into light harvesting for photosystem II in green algae. *Nat. Plants* **5**, 1320–1330 (2019).
15. Renger, T. Theory of excitation energy transfer: from structure to function. *Photosynth. Res.* **102**, 471–485 (2009)
16. Syski, R. *Passage Times for Markov Chains*. (IOS Press., 1992).
17. Asmussen, S. R. Markov Jump Processes. In: *Applied Probability and Queues*. Stochastic Modelling and Applied Probability **51**. 39–59 (2003).
18. Gagniuc, P. A. *Markov Chains: From Theory to Implementation and Experimentation* (John Wiley & Sons, New Jersey, 2017).
19. van der Weij-de Wit, C. D., Dekker, J. P., van Grondelle, R., van Stokkum, I. H. Charge separation is virtually irreversible in photosystem II core complexes with oxidized primary quinone acceptor. *J. Phys. Chem. A* **115**, 3947–3956 (2011).

20. Belgio, E., Johnson, M. P., Jurić, S., Ruban, A. V. Higher plant photosystem II light-harvesting antenna, not the reaction center, determines the excited-state lifetime-both the maximum and the nonphotochemically quenched. *Biophys. J.* **102**, 2761–2771 (2012).
21. Björkman, O. & Demmig, B. Photon yield of O₂ evolution and chlorophyll fluorescence characteristics at 77-K among vascular plants of diverse origins. *Planta* **170**, 489–504 (1987).
22. Pfündel, E. E. Action of UV and visible radiation on chlorophyll fluorescence from dark-adapted grape leaves (*Vitis vinifera* L.). *Photosynth. Res.* **75**, 29–39 (2003).
23. Papageorgiou, G. C. & Govindjee *Chlorophyll a Fluorescence: A Signature of Photosynthesis*. (Springer, Berlin, 2007).
24. Grinstead, C. M., Snell, J. L. Ch. 11: Markov Chains. *Introduction to Probability*. American Mathematical Society (1997).
25. Bharucha-Reid, A. T. *Elements of the Theory of Markov Processes and Their Applications* (McGraw-Hill, New York, 1960).
26. Lorenz, M. Methods of Measuring the Concentration of Wealth. *J. Am. Stat. Assoc.* **9**, 209–219 (1950).
27. Bellù, L. G., Liberati, P. Inequality Analysis – The Gini Index. *Food and Agriculture Organization*, United Nations. (2006).
28. van Grondelle, R. & Novoderezhkin, V. I. Energy transfer in photosynthesis: experimental insights and quantitative models. *Phys. Chem. Chem. Phys.* **8**, 793–807 (2006).
29. Ruban, A. V. et al. Identification of a mechanism of photoprotective energy dissipation in higher plants. *Nature* **450**, 575–578 (2007).
30. Ahn, T. K. et al. Architecture of a charge-transfer state regulating light harvesting in a plant antenna protein. *Science* **320**, 794–797 (2008).
31. Mazor, Y. Borovikova, A., Caspy, I., & Nelson, N. Structure of the plant photosystem I supercomplex at 2.6 Å resolution. *Nat. Plants* **3**, 17014 (2017).
32. Ishizaki, A., & Fleming, G. R. Quantum coherence in photosynthetic light harvesting. *Annu Rev. Condens Matter Phys* **3**, 333–361 (2012).

Acknowledgements

We gratefully acknowledge support from the National Fund of Science and Technology Development (FONDECYT grant no. 11190096 to H.K.) and Japan Society for the Promotion of Science (KAKENHI Grant-in-Aid 16H06553 to J.M.)

Author contributions

H.K. and E.K. conceived the study. E.K. constructed the data and H.K. conducted the analyses. J.M. provided resources and supervision. H.K. and E.K. prepared the manuscript. All four authors (H.K., E.K., M.A.V.-C. and J.M) interpreted the results and edited the manuscript.

Competing interest declaration

The authors declare no competing interests.

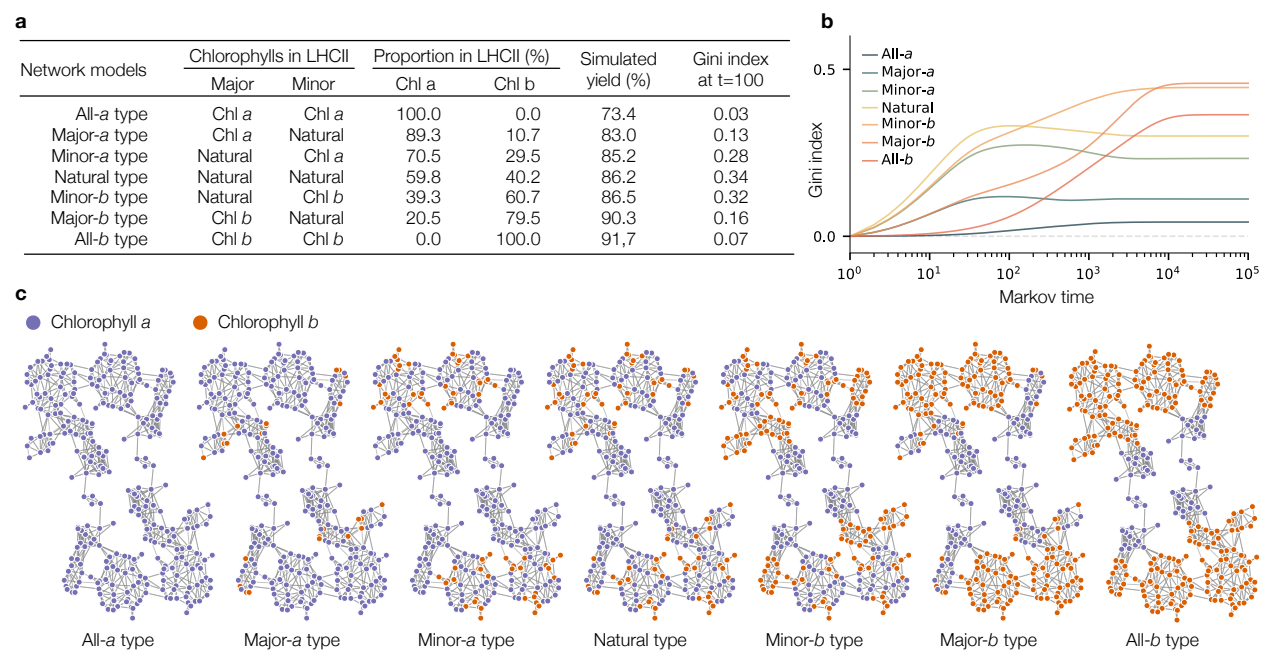
Additional Information:

Extended data is available for this paper.

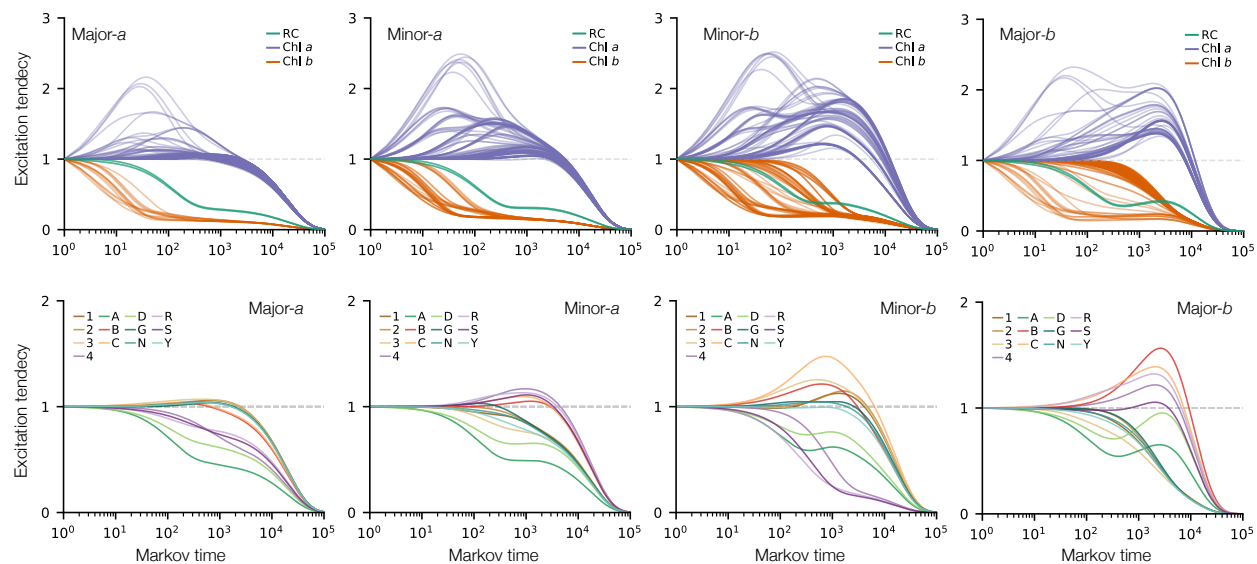
Reprints and permissions information is available at <http://www.nature.com/reprints>.

Correspondence and requests for materials should be addressed to H.K. and J.M.

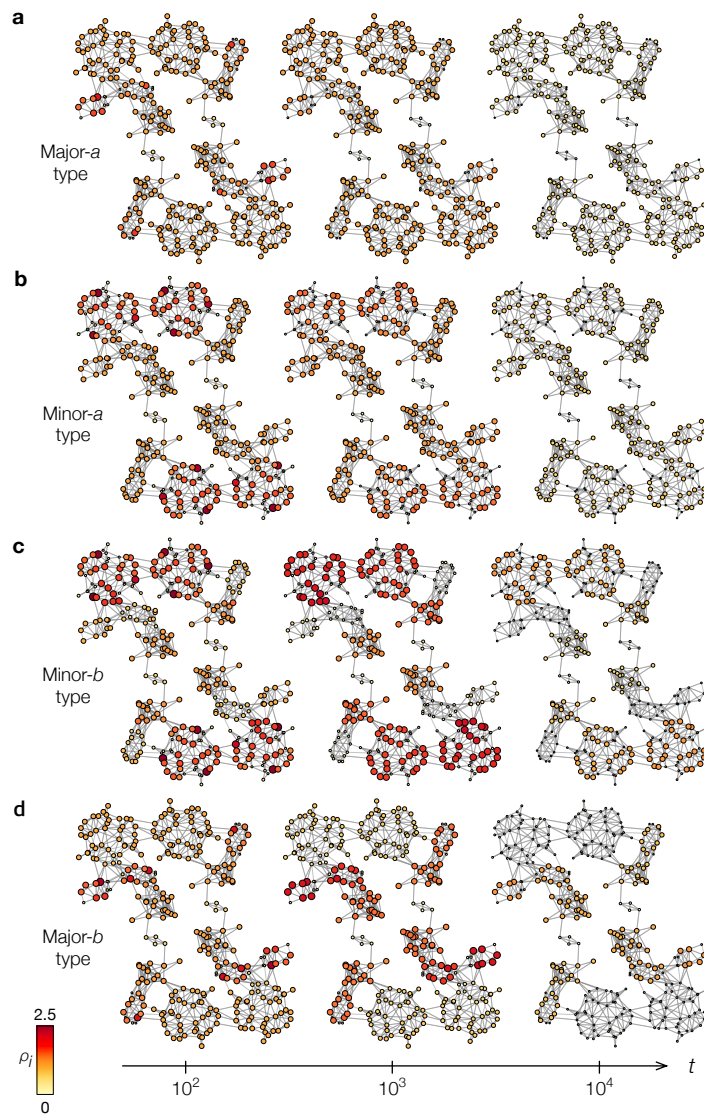
Extended Data



Extended Data Fig. 1 | The complete list of the PSII network models. The composition of each model is summarized in the table (a). The transition of the Gini index calculated from the excitation tendency of the Chls in each model shows different pattern between PSII network models (b). The natural PSII network reaches the largest Gini index at short time $t < 10^2$. The network visualization of the various PSII network models are in (c) illustrating the type of Chl with color. The links with the top 2% transition probability are shown for visual clarity.



Extended Data Fig. 2 | The excitation tendency transition of the four PSII network models. The transition patterns of the excitation tendency for Major-a, Minor-a, Minor-b, and Major-b models are shown in the upper panel by each Chls; in the lower panels by proteins.



Extended Data Fig. 3 | The excited energy transition in the four PSII networks models. The excitation tendency distribution at $t=10^2$, 10^3 , and 10^4 is shown for the models of Major-*a* (a), Minor-*a* (b), Minor-*b* (c), and Major-*b* (d).

We don't provide supplementary information